Investigating the Applicability of Modern Widely Tunable Lasers to Laser Heterodyne Radiometry for Atmospheric Composition Monitoring

Adela Collado-Rodríguez, Aldo Moreno-Oyervides, Omaira García, and Pedro Martín-Mateos

***Abstract*— Greenhouse gas emissions are widely recognized by the scientific community as the main cause of climate change. This has led to an enormous increase in interest in techniques for studying atmospheric composition over the last few decades. Laser heterodyne radiometry (LHR) systems represent one of the most promising alternatives for such studies, given their inherent characteristics, which have led to enormous progress in the last decades. Although these systems offer a wide range of advantages, the optical span is limited by the tuning range of the local oscillator laser, usually using distributed feedback (DFB) lasers, which limits the span to a few absorption lines. This has a negative impact on the performance of atmospheric gas concentration retrieval compared to the multitude of absorption lines retrieved by traditional Fourier Transform spectroscopy systems. In this context, the use of widely tunable lasers represents an optimal approach to greatly expand the range of LHR systems straightforwardly. This article presents the first comprehensive study of the applicability of state-of-the-art widely tunable lasers to LHR systems in a direct comparison of their performance, in all aspects of interest, with DFBs. The conclusions of this work prove that, although there are still a number of challenges to be addressed before widespread use, these sources demonstrate enormous potential and remarkable advantages.**

***Index Terms*— Gas sensing, laser heterodyne radiometry (LHR), optical sensing, widely tunable laser.**

I. Introduction

THE recognition that changes in the composition of the Earth's atmosphere are occurring, on both long and short timescales, thereby modifying our environment and climate, has resulted in scientific debate, as well as public concern in the last decades [1]. It is widely established that atmospheric emissions of greenhouse gases (hereinafter referred to as GHGs), primarily induced by human activities, are the main contributors to such changes and the observed global warming [2]. Additionally, GHG emissions entail other significant climate impacts. As a reference, as controlled ozone-depleting substances decline, recovery of the stratospheric ozone layer and its long-term evolution largely depend on GHG concentrations as key modulators of stratospheric temperatures [3, and references therein].

In this climate change scenario, accurate accounting of emissions and removals of carbon dioxide (CO_2), the most abundant and long-lived GHG, is critical for planning and verifying the emission reduction targets in support of the Paris Agreement [4]. To improve estimates of countries' carbon budgets and to better understand the physical and chemical processes involved, enhancing the existing observation networks with stable isotopologues of CO_2 (e.g., $14C_2$) and fossil fuel CO_2 co-emitted species measurements (e.g., carbon monoxide, nitrogen oxides, ammonia, etc.) across major CO_2 emitting regions is indispensable. These observations can play a pivotal role in helping to assess regional CO_2 emissions and to separate the atmospheric signals related to the different flux processes (i.e., biogenic and anthropogenic flux components) [5]. Nevertheless, as it is recognized by the last Green Report published by the European Commission CO_2 Monitoring Task Force [6], among others, the sparseness of current in situ atmospheric CO_2 measurement networks does not sufficiently constrain estimates of fossil anthropogenic emissions. This has led to the need for reinforcing CO_2 monitoring and related species, as well as a global interest in the development of techniques for the study of atmospheric gas composition.

At present, Fourier transform infrared (FTIR) [7] systems are the most widely recognized and utilized systems for accurate measurements of greenhouse gases in the atmosphere. FTIR systems for gas concentration measurements utilize an interferometer to analyze the infrared absorption spectra of molecules. Their main advantage is their greater optical span, which has a favorable effect on the performance of atmospheric gas concentration retrieval.

Laser heterodyne radiometry (LHR) [8], [9], [10], [11], [12], [13] is considered one of the best alternatives to both complement and improve the current observation systems, thanks to the technique characteristics, such as high optical resolution, flexibility of operation, and a compact instrument design. However, the main limitation of LHR systems is an optical span restricted by the tuning range of the local oscillator laser [a distributed-feedback (DFB) laser on most occasions, due to their excellent performance characteristics]. This usually

Received 10 October 2024; revised 21 February 2025; accepted 3 March 2025. Date of publication 18 March 2025; date of current version 10 April 2025. This work was supported by the Agencia Estatal de Investigación (Spain) under Grant TED2021-131695B-100. The Associate Editor coordinating the review process was Dr. Yuya Koyama. *(Corresponding author: Pedro Martín-Mateos.)*

Adela Collado-Rodríguez, Aldo Moreno-Oyervides, and Pedro Martín-Mateos are with the Electronics Technology Department, Universidad Carlos III de Madrid, Leganes, 28911 Madrid, Spain (e-mail: adcollad@pa.uc3m.es; aldmoren@ing.uc3m.es; pmmateos@ing.uc3m.es).

Omaira García is with the Izaña Atmospheric Research Center (IARC), State Meteorological Agency of Spain (AEMet), Santa Cruz de Tenerife, 38002 Canarias, Spain (e-mail: ogarciar@aemet.es).

Digital Object Identifier 10.1109/TIM.2025.3552381

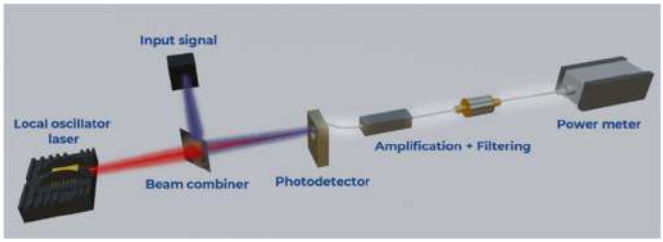

Fig. 1. Simplified diagram of LHR systems.

implies that the number of absorption lines analyzable with this measurement technique is limited to 3 or 4, with an unfavorable repercussion in the performance of atmospheric gas concentration retrievals [14]. So far, to overcome this, more than one local oscillator operates simultaneously [15], [16], [17], [18], which leads to an increase in both the cost and the complexity of the systems; nevertheless, covering a large number of absorption lines remains technically unfeasible. Given the current maturity of widely tunable lasers, such sources could soon become the best approach for enabling these spectral measurements over very wide ranges. On the other hand, these lasers are extremely sensitive to disturbances, which impose mechanical and thermal constraints when transporting the equipment and operating it in open environments due to exposure to atmospheric phenomena and temperature fluctuations [19]. However, advancements in technology are continually improving this aspect. Although the possible use of these sources has been raised previously [20], to the authors' knowledge, no conclusive study of its applicability to LHR has been published to date.

In this context, this article presents a comprehensive study of the applicability of modern, widely tunable lasers to LHR systems. Although this incorporation would increase the achievable optical span by several orders of magnitude, making it directly comparable to other existing atmospheric measurement techniques (such as FTIR systems), this work demonstrates that there are still several notable challenges that need to be addressed for this to be feasible.

II. Material and Methods

A. Laser Heterodyne Radiometry and Frequency Comb Calibration

With LHR, it is possible to retrieve, with very high optical resolution, the spectrum of an input optical signal. In LHR systems, the incoming signal is combined with the local oscillator laser, and the resulting beam is taken to a photodetector. The output of the photodetector provides a downshifted radio frequency (RF) copy of the spectrum of the optical input signal, which is amplified and filtered to configure the optical resolution of the radiometer. The RF power is then detected by an RF power meter, from which the spectrum of the optical signal is retrieved when the laser emission frequency is swept. A simplified diagram of an LHR system is shown in Fig. 1.

Additionally, one of the main aspects that needs to be considered in LHR systems is the frequency axis calibration. This is one of the major challenges of the technique and it is vital for an adequate absorption line characterization and, thus, atmospheric composition retrieval. To address this, the use

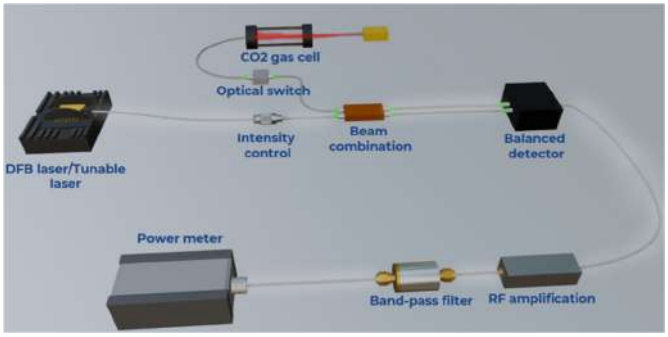

Fig. 2. LHR system implementation.

of an optical frequency comb as a frequency axis calibration method has been shown to achieve unprecedented levels of performance in the laboratory reaching sub-MHz frequency uncertainty [21]. Frequency comb calibration allows a portable high-accuracy option by providing a set of calibration marks as the teeth spacing. The accuracy of these can be less than 1 ppm, leading to a high level of performance. When an optical frequency comb is connected to the input of the LHR system, the position (separation) of all the teeth of the comb can be straightforwardly identified and stored allowing frequency calibration at the same time measurements are being made. Hence, after the proper processing, an accurate frequency axis determination is achieved. Similarly, in a previous publication [22], the first deployable frequency comb was also described and evaluated. This latter comb generation method is utilized in this study to evaluate the performance of the different laser sources employed with respect to frequency sweep accuracy.

B. Instrument Design and Implementation

For this study, an LHR system was implemented with the architecture shown in Fig. 2. In this system, the incoming optical signal is intensity modulated via a fiber optical switch (OSW12-1310-S, Thorlabs). The local oscillator laser, swept over the optical span to analyze, is attenuated to avoid the detector saturation and then combined with the input signal via a 2 by 2 fiber coupler. The combined optical signal reaches an amplified balanced detector (PDB470C-AC, Thorlabs), where both optical signals are mixed. The resulting heterodyned signal is amplified, filtered, and then detected by an USB power sensor (U2041XA, Keysight), which provides a digitized reading of the RF signal power. The signal is amplified via ASC118C amplifier (Amplifier Solution Corporation). Subsequently, two filters are employed, a high-pass filter SHP-20+ (Mini-Circuits) and a low-pass filter SLP300+ (Mini-Circuits). The objective of these filters is to minimize the influence of laser noise and to set the optical resolution to 0.02 cm^{-1}, which is the standard resolution employed for ground-based remote sensing networks for GHG monitoring [23].

As anticipated in Section I, this study aims to evaluate the usability of the widely tunable laser for LHR; therefore, different laser sources are evaluated. Then, a high-performance widely tunable laser (CTL 1550 Toptica [24]), tunable between 1530 and 1620 nm, is compared against a DFB laser, which

is very commonly employed in current LHR implementations (EPI1570-DM, Eblana Photonics). In a similar manner to the study conducted with this widely tunable laser (and its spectral range), the system architecture and procedure apply to any other source of a comparable nature. It should be noted that the attenuation of both sources has been adjusted so that the average power is equalized, thereby ensuring a fair comparison between the two sources. To ensure maximum consistency and representativeness of results, in this study, all measurements have been carried out in the controlled environment of an instrumentation laboratory. Accordingly, sunlight has been replaced by a super luminescent diode emitting at 1550 nm (S5FC1005S, Thorlabs) followed by a gas cell, with an optical path length of 80 cm and filled with 100% CO_2 (see Fig. 2) to introduce absorption features. The system is controlled, and measurements are achieved using a self-developed LabVIEW virtual instrument. Before taking measurements, the number of points for each measurement and the integration time per point are set. The laser intensity is translated to a corresponding voltage and a sweep is performed, creating the required sweep in the wavelength. In the case of the widely tunable laser, the sweep is controlled by the laser itself to not influence the measurement in any way.

III. Results and Discussion

Throughout this study, a series of tests were performed to evaluate the feasibility of using arguably one of the best performing, commercially available widely tunable lasers to date, the CTL 1550 from Toptica, for LHR and to compare it with a regularly employed source in these systems, such as the ubiquitous DFB laser. To facilitate a direct comparison in terms of performance and usability, a very relevant part of the study focuses on a 1 nm or 3 cm^{-1} spectral window located at around 1570.2–1571.2 nm, where three CO_2 absorption lines corresponding to the central wavelengths of 1570.54, 1570.83, and 1571.11 nm are present. The 80-cm cell, filled with 100% CO_2, provides weak absorption lines compared to typical atmospheric absorptions at the operating wavelength, allowing a more detailed and visual comparison of the performance between the two laser sources. In all the tests, both lasers were configured so that the number of points per measurement and the scanning time were the same. In Sections III-A–III-C, the power characteristics, the wavelength consistency, and the spectral measurement capabilities of the lasers are presented and discussed.

A. Raw Measurements and Power Characteristics of the Laser Sources

In the first tests performed, the power characteristics of the lasers and several raw measurements were analyzed. Both sources were centered in the 1-nm spectral window introduced above. The integration time per point for both sources was set to 400 ms to minimize the influence of noise in the comparative study. A total of five full sweeps of 370 points (for both laser sources) were employed for this comparison. This number of points is 50% higher than the number of points provided in the standard configuration of atmospheric

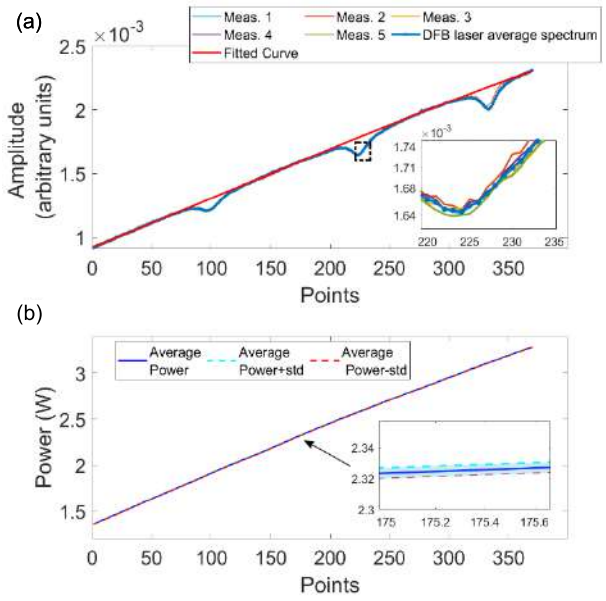

Fig. 3. (a) Average spectrum measured with the DFB laser (blue) and baseline adjustment (red). (b) Average power sensor measurement for the DFB laser and its standard deviation.

characterization systems [23]. This allows a more accurate characterization of the performance of the evaluated sources.

Figs. 3(a) and 4(a) shows the averaged measurements taken by the LHR system working with the DFB laser and the widely tunable laser, respectively, along with their corresponding power measurements [Figs. 3(b) and 4(b)] (provided by the monitor output of the photodetector). In both figures, the three CO_2 absorption lines can be clearly identified; however, the measurement baseline, associated with the power profile of the laser, shows huge differences. Although the DFB laser presents a greater, but much flatter, change in the output power profile, the response of the widely tunable laser is strongly dominated by power ripples. The power output during the scan was also quantified and characterized using a power meter external to the system. The measurements obtained were found to be consistent, which corroborates the power profile while sweeping the two laser sources. The widely tunable laser presents, therefore, a far more challenging baseline to characterize and compensate. As a matter of fact, with the widely tunable laser, it is necessary to perform an eighth-order sum of sines fitting [Fig. 4(a) in red] for a proper baseline removal. It is important to note that the amplitude variation matches the power variation [Fig. 4(b)]. Therefore, we can state that this behavior is not due to system inconsistent detection inconsistencies, but because the laser power itself exhibits variability during the scanning process at different wavelengths. The variability is illustrated in Fig. 4(a), which displays the five measurements utilized to calculate the mean spectrum, along with the averaged spectrum (in blue) and the fit curve (in red). To determine the extent of variability between scans, the average standard deviation of the difference of each scan with respect to the average spectrum was calculated. This resulted in an average difference of 7.16×10^{-7} for the DFB laser and 8.32×10^{-7} for the widely tunable laser. It could be argued that one potential method for addressing this challenge is through optical power stabilization, a technique

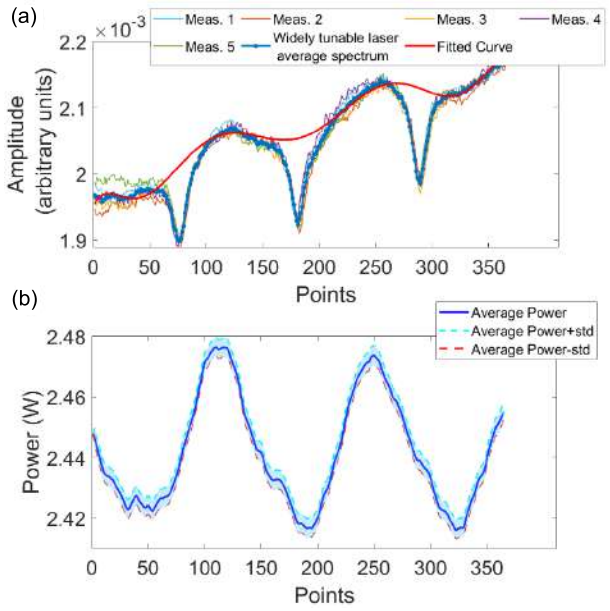

Fig. 4. (a) Average spectrum measured with the widely tunable laser (blue) and baseline adjustment (red). (b) Average power sensor measurement for the widely tunable laser and its standard deviation.

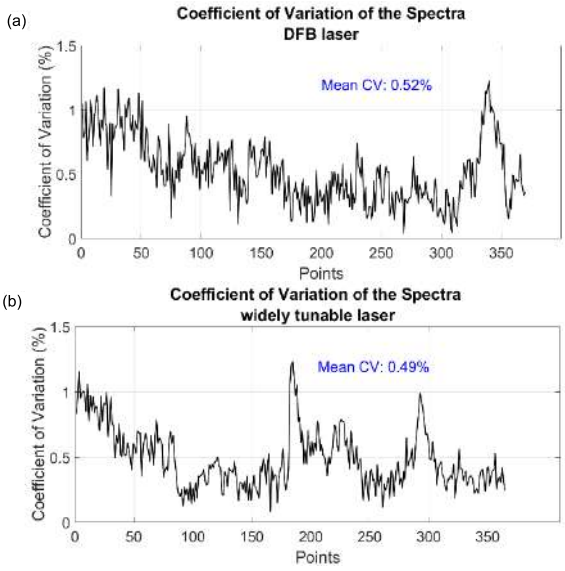

Fig. 5. (a) CV for the spectrum measured with the DFB laser. (b) CV for the spectrum measured with the widely tunable laser.

that has been previously validated in [21]. However, this kind of power stabilization might have a strong influence on the signal-to-noise ratio (SNR). On the other hand, a simple third-order linear fit can be used to accurately fit and remove the baseline for the DFB laser measurements.

The coefficient of variability (CV) has been calculated to study the variation between spectra. The CV is a relative measure, which compares the standard deviation and the average spectrum providing a quantitative representation of the variation present in the data. Fig. 5(a) and (b) shows the CV as a percentage point by point for each source. The mean CV for the measurements is also shown. In no instance did the proportion exceed 1.25%, and an average of approximately 0.5% was ascertained, thereby evidencing the minimal variation between each sweep.

B. Wavelength Linearity, Accuracy, and Consistency

In LHR experiments, besides an adequate intensity characterization, it is vital to have an accurate wavelength axis. Methods such as the use of etalons have been widely employed for this application. Nevertheless, recent technological developments have allowed the use of wavelength calibration based on optical frequency combs [21], [22]. Even though, in principle, both methods are equivalent, the accuracy and repeatability provided by frequency combs, in which the repetition rate can be referenced to a frequency standard, is noticeably superior.

In this study, an optical frequency comb signal has been generated to characterize and calibrate this feature of the instrument and also to analyze the final sweep characteristics with high precision. The wavelength calibration process consists of two steps: 1) identifying the position of the teeth of the comb in the measurement span and 2) extracting the positions of the teeth for the subsequent calculation of the performance and/or the wavelength correction polynomial. This allows for a complete rearrangement of the frequency axis, which, in turn, enables the calibration marks (teeth) to be perfectly aligned with the characteristics of the reference frequency comb, hence compensating for any nonidealities in the frequency axis of the measurement.

In this case, and covering the above-identified 1-nm bandwidth, an optical frequency comb with a repetition rate of 10 GHz has been generated and used to characterize and calibrate the frequency axis in the measurements with the two laser sources. As a fundamental difference to previous measurements, 3000 points were used in this experiment, ensuring the representativeness of the results. Since the teeth of the comb can be considered to be perfectly evenly spaced, the accuracy of the frequency axis retrieved from both sources will be assessed by analyzing the interdistance error between the teeth in the measurements using the calibration comb signal. In this article, this will be calculated as the standard deviation of the interdistances between each pair of adjacent teeth in the comb. A Gaussian curve is fit to each tooth to obtain the center point, which corresponds to the position of the tooth within the measurement data vector. Thus, this metric yields a very price characterization of the accuracy of the wavelength axis. A fifth-order fitting was employed for a better performance. A measurement obtained for the widely tunable laser is shown in Fig. 6. With this source, the teeth of the comb are very evenly distributed, with an error of 0.52 pm (0.0020 cm^{-1} and 60 MHz), demonstrating that the frequency control is highly refined. This high level of linearity and accuracy means that it can be used directly in most applications without additional corrections.

On the contrary, as evidenced in Fig. 7(a), with the DFB laser, the system does not provide inherently an equispaced distribution of the teeth (the graph illustrates a slightly greater spacing between the teeth on the left side than those on the right side). This makes the use of some frequency correction mechanisms mandatory when using DFB lasers. Quantitatively, an initial spacing error of 8.8 pm (0.0352 cm^{-1}

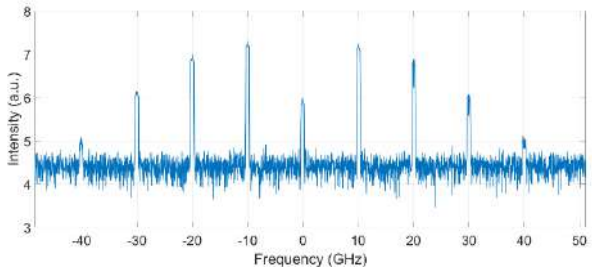

Fig. 6. Widely tunable laser frequency comb.

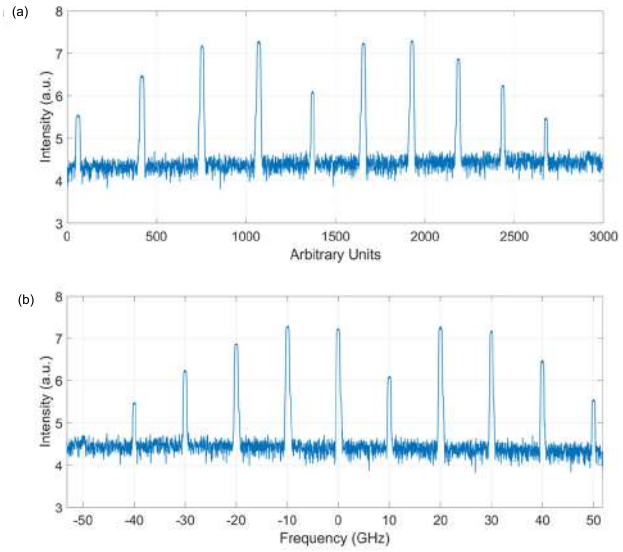

Fig. 7. (a) DFB laser frequency comb before frequency axis calibration. (b) DFB laser frequency comb after frequency axis calibration.

and 1050 MHz) is encountered, almost two orders of magnitude worse than with the previous laser. Nevertheless, an axis correction based on wavelength axis calibration using the frequency comb can be straightforwardly applied. This procedure, covered in detail in [22], results in highly accurate results, with a resulting error of only 0.14 pm (0.0006 cm^{-1} and 18 MHz). This value is significantly higher than that obtained with the widely tunable laser, which may be of great importance for the processing of atmospheric absorptions. The new wavelength axis-corrected measurement is shown in Fig. 7(b).

A further study of the consistency of the wavelength sweep can be conducted using a single-frequency comb teeth analysis. Regardless of the sweep linearity offered by each laser source, the consistency and ability to maintain small, but very uniform increments in the wavelength sweep, is another highly desirable feature of lasers for LHR. The results of a comparison of the two sources are shown in Fig. 8, in which three very representative measurements of different teeth of the comb are shown after spectral analysis with the two laser sources. The results obtained can be analyzed from different perspectives. On the one hand, it can be seen that the scanning stability of the DFB laser is clearly superior, with intensity values that increase or decrease monotonically during the scanning of the tooth and spectral measurements that are very consistent across all teeth. On the other hand, despite its good linearity, the widely tunable laser shows slightly erratic frequency deviations when the analysis is performed at such a high optical resolution, which is reflected in the

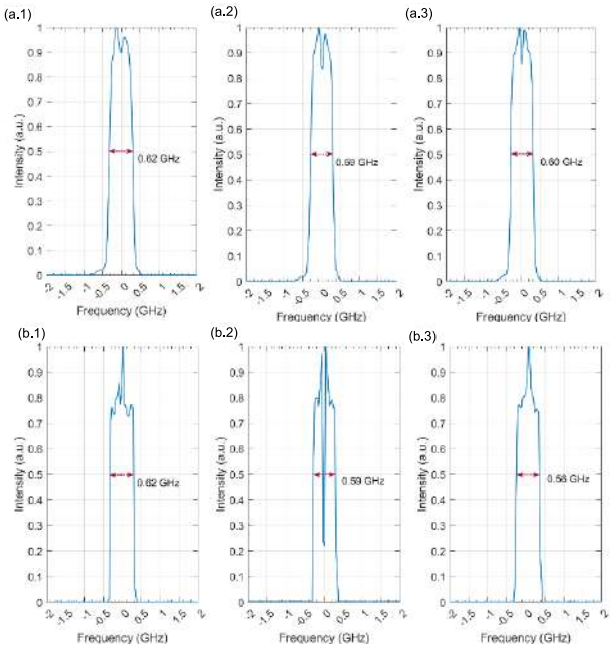

Fig. 8. (a.1)–(a.3) Normalized frequency comb teeth for the DFB laser. (b.1)–(b.3) Normalized frequency comb teeth for the widely tunable laser.

discrepancies shown in the measurements. This is evidence of the superior performance of the DFB laser in this aspect of the operation of the system. However, the ideal double sideband spectrum of LHR systems, which should be 40 MHz in our implementation, is only clearly reconstructed by the widely tunable laser, which indicates its narrower linewidth. However, this is something that cannot be consistently achieved with the font used, and there is a probability, which in our case is close to 40%, that the scanning performed is not fine enough to be able to display in the center notch. As far as the full-width at half-maximum (FWHM) of the teeth is concerned, the differences in the linewidth of the lasers are so small that no significant differences can be seen. Additionally, this is not an aspect of great importance in LHR, since, in both cases, the linewidth of the laser is well below the width of the spectral line to be analyzed.

C. Spectral Measurement Capabilities

Among the different parameters assessed in this section, the SNR is the first to be addressed. This SNR is obtained, for both laser sources, as the standard deviation of the intensity detected in regions without significant absorptions (an additional fitting is used to ensure that small deviations from the baseline do not influence the SNR calculation). The spectra utilized in this investigation, as measured with both the DFB laser and the widely tunable laser, are represented in blue in Figs. 9(a) and 10(a), respectively, and are the result of the application of the baseline removal and wavelength correction procedures described in the previous sections. The spectral span goes from 6364.5 to 6367.5 cm^{-1} (1570.5–1571.2 nm). To calculate the SNR, the standard deviation of the regions devoid of absorption [around 6365.3 and 6366.8 cm^{-1}; Figs. 9(a) and 10(a), in green] in both cases was considered. This value was found to be 0.0010 for the DFB laser and 0.0015 for the widely tunable laser, for SNRs of 1000 and 666, respectively. The slightly better performance of the DFB laser is undoubtedly a

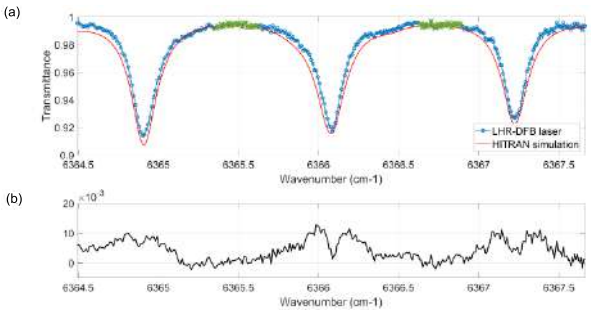

Fig. 9. (a) Comparison of average spectrum measured with DFB laser after baseline compensation and axis correction (blue) and HITRAN simulation (red). (b) Residual error (measurement-simulation).

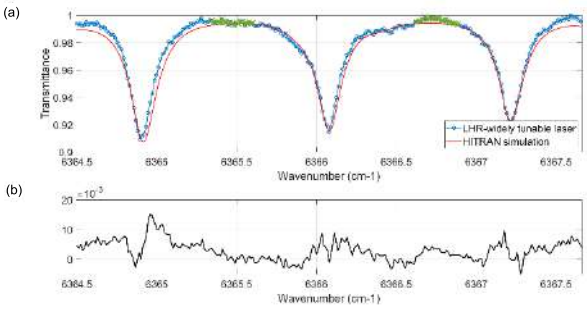

Fig. 10. (a) Comparison of average spectrum measured with the widely tunable laser after baseline compensation and axis correction (blue) and HITRAN simulation (red). (b) Residual error (measurement–simulation).

direct result of its superior intensity versus wavelength characteristics compared to the widely tunable laser (as analyzed in Section III-A). This experiment has been performed for a power level of 1 μW at the input of the system, a value comparable to that obtained when a collimator is used to collect sunlight.

Additionally, once both the baseline and the wavelength axis have been corrected, it is now possible to make a direct comparison between measured spectra and a reference spectrum simulated using the HITRAN 2020 database [25], [26]. Fig. 9(a) displays the corrected average spectrum for the DFB laser in blue, and the simulated transmittance spectrum for 100% CO_2 concentration along an 80-cm-long gas cell in red. Analogously, the results obtained for the widely tunable laser are shown in Fig. 10(a).

On the other hand, Figs. 9(b) and 10(b) displays the residual error, where it can be seen that small differences in line depths between the measured and simulated spectra result in greater errors in the absorption zones compared to the nonabsorption regions. These spectral discrepancies are likely to be due to the baseline adjustment and minor wavelength inconsistencies but also to the assumed purity of the CO_2 concentration in the cell. As a measure of error, the standard deviation of the residuals yields very similar values: 0.0038 for the DFB laser and 0.0034 for the widely tunable laser. This demonstrates that both sources offer closely aligned spectral reconstruction performance after baseline adjustments and axis calibration.

D. Full Scan

Finally, and after having presented the very comprehensive comparison with the DFB laser performance within its tuning range, we evaluate the possible use of the widely tunable laser

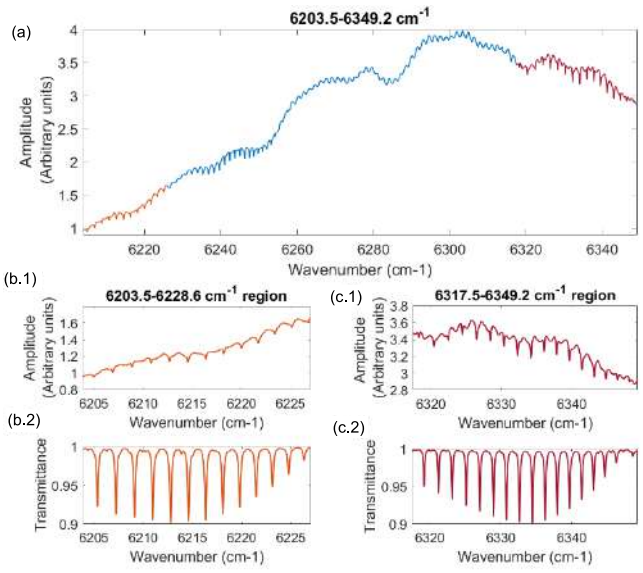

Fig. 11. (a) 6349.2–6203.5 cm^{-1} scan region. (b.1) 6203.5–6228.6 cm^{-1} scan region. (b.2) 6203.5–6228.6 cm^{-1} HITRAN simulation. (c.1) 6317.9–6349.2 cm^{-1} scan region. (c.2) 6317.9–6349.2 cm^{-1} region HITRAN simulation.

for wide spectral span LHR measurements. On this occasion, the measurements extend for 90 nm or 400 cm^{-1}, two orders of magnitude greater than that allowed by the DFB laser (without temperature changes in this device). Fig. 11(a) shows the raw data obtained from a scan over almost the entire widely tunable laser range (6349.2–6203.5 cm^{-1}). Although the complete scan extends from 1530 to 1620 nm (6535.9–6172.8 cm^{-1}), the extremities have been trimmed to enhance the visibility of the lines present within the full scan. This scan reveals the presence of numerous absorption lines, primarily due to the CO_2 absorption and its main isotopologues in the regions between approximately 6325–6375 cm^{-1} and 6200–6250 cm^{-1}, and proves the possibility of detecting all these molecular resonances with a single device as a light source. Fig. 11(b.1) and (c.1) displays some of these lines along with the HITRAN simulation in Fig. 11(b.2) and (c.2), which corroborates the potential of the full scan. However, the main challenge in extracting spectral information from the measurement of the full sweep of the broadly tunable laser is the enormous variability of the optical power emitted by the laser source. This makes it very difficult to apply automated full-span adjustments that allow the spectral response of the atmosphere to be extracted with little effort. However, the promising results obtained in previous analyses in the 1-nm range confirm that, after a proper characterization of the baseline, these procedures could be extended to the complete scanning range with appropriate development.

IV. Conclusion

This study presents, to the authors' knowledge, the first comprehensive comparative work on the performance of a state-of-the-art, widely tunable laser compared to a DFB laser for use in LHR. As demonstrated by all the studies performed in the 1-nm range, both sources show great potential for future operational implementation in LHR systems. Although state-of-the-art, widely tunable laboratory sources still have some

notable disadvantages, such as higher intensity fluctuations and less precise wavelength sweep control, the results obtained point to that they can offer performance comparable to that of the DFB for LHR. We can highlight some advantages beyond the higher span, such as wavelength accuracy. Nevertheless, in the present study, the main limitation of these sources has been the variability in the power observed during the sweep, a common phenomenon observed in this type of source, which is a major challenge in baseline compensation. However, it has been shown that in small spectral ranges, it is feasible to eliminate this problem in a not-too-labor-intensive way.

For all the above reasons, we believe that the main challenge nowadays in the practical and operational application of these sources to LHR systems inside and outside the laboratory lies in their dimension and cost. On the one hand, the size of these lasers is significantly larger than that of a standard LHR system. On the other hand, the high cost of these units poses a major challenge when aiming to establish dense monitoring networks to enhance our understanding of GHG emissions and other important atmospheric compounds. Despite their lower span, DFB lasers are far more convenient in both size and cost. High-performance widely tunable lasers are priced at an order of magnitude higher than DFB lasers. However, they enable a span of up to 100 times greater with the drawback of increased complexity. Although DFBs have been utilized in the field with no reported issues, widely tunable lasers are equipped with mirrors and mechanical components that require highly precise alignment.

In summary, despite the various challenges that widely tunable sources still present to date, the current work demonstrates that these laser sources have enormous potential and are a very encouraging option for extending the measurement range, and thus multiplying the capabilities, of the LHR systems of the future.

REFERENCES

[1] M. Gottwald et al., *SCIAMACHY, Monitoring the Changing Earth's Atmosphere*. Weßling, Germany: DLR, Institute für Methodik der Fernerkundung, 2006.

[2] IPCC, "Climate change 2022—Impacts, adaptation and vulnerability: Working group II contribution to the sixth assessment report of the intergovernmental panel on climate change," Switzerland, Jun. 2023, doi: 10.1017/9781009325844.

[3] O. E. García et al., "Twenty years of ground-based NDACC FTIR spectrometry at Izaña observatory—Overview and long-term comparison to other techniques," *Atmos. Chem. Phys.*, vol. 21, no. 20, pp. 15519–15554, Oct. 2021, doi: 10.5194/acp-21-15519-2021.

[4] B. Byrne et al., "National CO_2 budgets (2015–2020) inferred from atmospheric CO_2 observations in support of the global stocktake," *Earth Syst. Sci. Data*, vol. 15, no. 2, pp. 963–1004, Mar. 2023, doi: 10.5194/essd-15-963-2023.

[5] B. Matthews, O. E. G. Rodríguez, E. C. Agulló, W. Spangl, and M. P. C. Lobera. *Arcimis: Report on How EIONET and EEA can Contribute to the Urban in Situ Requirements of a Future Copernicus Anthropogenic CO_2 Observing System*. Accessed: Oct. 2, 2024. [Online]. Available: https://repositorio.aemet.es/handle/20.500.11765/12594

[6] B. Pinty et al., "An operational anthropogenic CO_2 emissions monitoring & verification support capacity: Needs and high level requirements for in situ measurements," Eur. Commission Joint Res. Center, Tech. Rep., 2019. [Online]. Available: https://data.europa.eu/doi/10.2760/182790

[7] Z. Bacsik, J. Mink, and G. Keresztury, "FTIR spectroscopy of the atmosphere. I. Principles and methods," *Appl. Spectrosc. Rev.*, vol. 39, no. 3, pp. 295–363, Dec. 2004, doi: 10.1081/asr-200030192.

[8] R. T. Menzies and M. S. Shumate, "Air pollution: Remote detection of several pollutant gases with a laser heterodyne radiometer," *Science*, vol. 184, no. 4136, pp. 570–572, May 1974, doi: 10.1126/science.184.4136.570.

[9] E. L. Wilson, "A low-cost miniaturized laser heterodyne radiometer (mini-LHR) for near-IR measurements of CO_2 and CH_4 in the atmospheric column," in *Proc. Conf. Lasers Electro-Opt. (CLEO)*, San Jose, CA, USA, Jun. 2016, pp. 1–2.

[10] D. Weidmann, T. Tsai, N. A. Macleod, and G. Wysocki, "Atmospheric observations of multiple molecular species using ultra-high-resolution external cavity quantum cascade laser heterodyne radiometry," *Opt. Lett.*, vol. 36, no. 11, p. 1951, Jun. 2011, doi: 10.1364/ol.36.001951.

[11] A. D. Sappey, B. P. Masterson, and J. Howell, "Development of a laser heterodyne radiometer for regional methane leak detection," *Appl. Opt.*, vol. 61, no. 10, p. 2697, Apr. 2022, doi: 10.1364/ao.440200.

[12] T. Wei et al., "Ground-based remote sensing of CO_2 in the atmospheric column using a portable laser heterodyne radiometer with a balanced photodetector," in *Proc. Conf. Lasers Electro-Opt. Eur. Eur. Quantum Electron. Conf. (CLEO/Europe-EQEC)*, Munich, Germany, Jun. 2023, p. 1, doi: 10.1109/cleo/europe-eqec57999.2023.10232594.

[13] M. M. Flores, D. S. Bomse, A. L. Gomez, and J. H. Miller, "Deployment of ground-based LHR sensor for greenhouse gas vertical profile measurements," in *Proc. CLEO*, San Jose, CA, USA, 2023, pp. 1–2.

[14] A. Moreno-Oyervides, O. Bonilla-Manrique, O. E. García, A. Collado-Rodríguez, and P. Martín-Mateos, "Towards the next generation of sensors for surveying the atmospheric carbon cycle: A new laser heterodyne radiometer for CO_2 monitoring," in *Proc. NDACC-IRWG/TCCCON/COCCON Annu. Meeting*, Boulder, CO, USA, Jul. 2024, pp. 8–12.

[15] G. Wang et al., "Simultaneous remote sensing of multiple atmospheric gases (CO_2, CH_4, and H_2O) based on an all-fiber laser heterodyne spectroradiometer," *Appl. Phys. B, Lasers Opt.*, vol. 129, no. 8, Aug. 2023, doi: 10.1007/s00340-023-08071-2.

[16] J. Wang et al., "Ultra-high resolution portable dual-channel laser heterodyne radiometer," *IEEE Trans. Instrum. Meas.*, vol. 73, 2024, Art. no. 7007609, doi: 10.1109/TIM.2024.3420357.

[17] H. Deng et al., "Development of a laser heterodyne spectroradiometer for high-resolution measurements of CO_2, CH_4, H_2O and O_2 in the atmospheric column," *Opt. Exp.*, vol. 29, no. 2, p. 2003, Jan. 2021, doi: 10.1364/oe.413035.

[18] J. Wang et al., "A fibered near-infrared laser heterodyne radiometer for simultaneous remote sensing of atmospheric CO_2 and CH_4," *Opt. Lasers Eng.*, vol. 129, Jun. 2020, Art. no. 106083, doi: 10.1016/j.optlaseng.2020.106083.

[19] V. Weldon, D. McInerney, R. Phelan, M. Lynch, and J. Donegan, "Characteristics of several NIR tuneable diode lasers for spectroscopic based gas sensing: A comparison," *Spectrochimica Acta A, Mol. Biomolecular Spectrosc.*, vol. 63, no. 5, pp. 1013–1020, Apr. 2006, doi: 10.1016/j.saa.2005.10.051.

[20] J. Wang et al., "External-cavity diode laser-based near-infrared broadband laser heterodyne radiometer for remote sensing of atmospheric CO_2," *Opt. Exp.*, vol. 31, no. 6, p. 9251, Mar. 2023, doi: 10.1364/oe.482131.

[21] C. Fredrick, F. Olsen, R. Terrien, S. Mahadevan, F. Quinlan, and S. A. Diddams, "Thermal-light heterodyne spectroscopy with frequency comb calibration," *Optica*, vol. 9, no. 2, p. 221, Feb. 2022, doi: 10.1364/optica.440389.

[22] A. Moreno-Oyervides, O. E. Bonilla-Manrique, O. García, and P. Martín-Mateos, "Design and evaluation of a portable frequency comb-referenced laser heterodyne radiometer," *Opt. Lasers Eng.*, vol. 171, Dec. 2023, Art. no. 107801, doi: 10.1016/j.optlaseng.2023.107801.

[23] D. Wunch et al., "Comparisons of the Orbiting Carbon Observatory-2 (OCO-2) XCO_2 measurements with TCCON," *Atmos. Meas. Techn.*, vol. 10, no. 6, pp. 2209–2238, Jun. 2017, doi: 10.5194/amt-10-2209-2017.

[24] R. Neuhaus, "TOPTICA photonics, Inc.: Simple operation of a continuously tunable laser with up to 120 nm mode-hop free tuning range," *Proc. SPIE*, vol. 11716, Mar. 2021, Art. no. 117162C, doi: 10.1117/12.2596080.

[25] I. E. Gordon et al., "The HITRAN2020 molecular spectroscopic database," *J. Quantum Spectrosc. Radiat. Transf.*, vol. 277, Sep. 2021, Art. no. 107949, doi: 10.1016/j.jqsrt.2021.107949.

[26] L. S. Rothman et al., "The HITRAN molecular spectroscopic database: Edition of 2000 including updates through 2001," *J. Quant. Spectrosc. Radiat. Transf.*, vol. 82, nos. 1–4, pp. 5–44, Nov. 2003, doi: 10.1016/s0022-4073(03)00146-8.